

Fast fluorescence dynamics in nonratiometric calcium indicators

M. Gersbach,¹ D. L. Boiko,^{1,2,*} C. Niclass,¹ C. Petersen,¹ and E. Charbon¹

¹Ecole Polytechnique Fédérale de Lausanne, Quantum Architecture Group, 1015, Lausanne, Switzerland

²Centre Suisse d'Electronique et de Microtechnique SA, 2002, Neuchâtel, Switzerland

(Dated: May 23, 2022)

A fluorescence decay of high-affinity non-ratiometric Ca^{2+} indicator Oregon Green BAPTA-1 is analyzed with unprecedented temporal resolution in the two-photon excitation regime. A triple exponential decay is shown to best fit the fluorescence dynamics of OGB-1. We provide a new model for accurate measurements of the free Ca^{2+} concentration and dissociation constants of non-ratiometric calcium indicators.

Fluorescence Lifetime Imaging Microscopy (FLIM) is used to locally probe the chemical environment of fluorophores, e.g., ion concentration, pH or oxygen content.^{1,2} To acquire time-resolved fluorescence images, the technique of Time-Correlated Single Photon Counting (TCSPC)³ in combination with detectors exhibiting single-photon sensitivity^{4,5} is commonly used enabling the photon time of arrival distribution to be measured with very high accuracy, insensitive to instabilities of the excitation beam intensity. So far, the temporal resolution of a few hundreds ps was considered sufficient in bio-medical FLIM applications.

In this letter, using a TCSPC system of 79ps resolution based on CMOS Single Photon Avalanche Diode (SPAD) detector technology, we measure the fluorescence decay of the high-affinity Ca^{2+} indicator Oregon Green BAPTA-1 (OGB-1) under two-photon excitation conditions. Our measurements reveal a fast dynamic behavior of OGB-1 fluorescence. We provide a model and a detailed comparison with previously reported data,^{1,7,8} which are acquired using a Photomultiplier Tubes (PMTs) with temporal resolution of 200ps. On example of OGB-1, we show that triple-exponential decay enables accurate measurements of the calcium concentration and dissociation constants of non-ratiometric fluorescent probes.

The SPAD-based TCSPC system is depicted in Fig.1. Our SPADs⁶ are integrated in a 32x32 array and incorporate on-chip high bandwidth I/O circuitry. The active region of a SPAD pixel [Fig.1(b)] consists of a p^+-n diode operating in the Geiger mode. Due to a small diameter (7 μm), our SPADs show an extremely low dark count rate (less than 10 Hz at room temperature). The single photon detection probability is 25 % at 500 nm wavelength, while the dead time is 25 ns with negligible afterpulsing (< 0.1 %).

Fluorescent molecules are excited in the two-photon

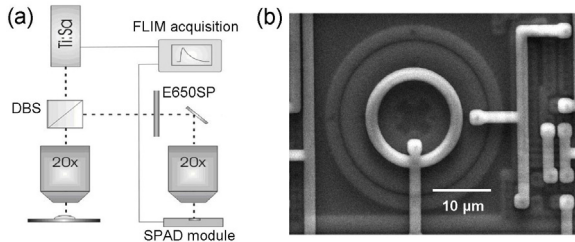


FIG. 1: (a) Schematic of the experimental setup for fluorescence lifetime measurements. (b) Scanning electron microscope image of a SPAD

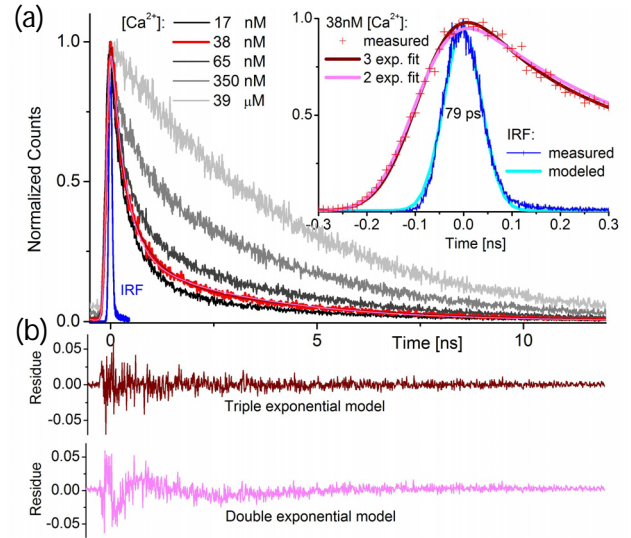


FIG. 2: (Color online) (a) Measured fluorescence decay of OGB-1 in the presence of various calcium concentrations (gray scale curves) and hyper-Rayleigh scattering from colloidal gold particles used to measure the IRF (blue curve). The red curve highlights measured fluorescence decay in a 38 nM free Ca^{2+} concentration buffer and the numerical fits of the double- (magenta) and triple-exponential (wine curve) decay models. The inset shows a close-up of the initial interval of 600ps width and (b) shows the residues for the two models.

regime,¹⁰ using a mode-locked Ti:Sapphire laser (MaiTai, Spectra Physics) emitting 100 fs optical pulses at 800 nm wavelength [Fig.1(a)]. The attenuated beam of 9 mW power is focused on a sample using a 20x microscope objective (XLUMPlanFL, Olympus), which also serves to collect the fluorescent emission. Fluorescence from OGB-1 samples treated here (central emission wavelength 520 nm) is directed towards the SPAD by a dichroic beam splitter (DBS) and a filter (E650SP, Chroma Technology) that suppress backscattered excitation pulses. Another 20x objective images the emission spot onto the SPAD. The low quantum yield of the two-photon excitation fluorescence and mismatch between the SPAD sensitive area (40 μm^2) and the fluorescent spot image result in a count rate at the detector of 10 kHz for 80 MHz repetition rate of excitation pulses. Respectively, the time discrimination is performed in a "reversed start-stop" configuration by measuring the time intervals from a photo-detection event at the SPAD to emission of a successive laser pulse. For pre-

cise timing of photon arrivals, we use a 6 GHz bandwidth oscilloscope (WaveMaster, LeCroy) incorporating a time-to-digital-converter (TDC) and enabling to compute histograms of photon arrivals.

Fig.2(a) shows the Instrument Response Function (IRF) of the entire system at 400 nm wavelength (blue curve). It is recorded by measuring the hyper-Rayleigh scattering of 800 nm wavelength pulses in a solution of colloidal gold particles (G1652, Sigma-Aldrich).¹¹ At the incident power of 90 mW, the average count rate of the detector is just 600 Hz. The measured photon arrival time jitter of 79 ps (FWHM) is dominated by the SPADs time-response characteristics. The IRF is only slightly asymmetrical and assumes a Gaussian-curve approximation $\text{IRF} = \exp(-t^2/2\sigma_{\text{IRF}}^2)$ (inset, cyan curve).

Fluorescent samples were composed of 2 μl OGB-1 dye (O6806, Molecular probes) and 20 μl Ca-EGTA buffer solutions from the calibration kit (C3008MP, Molecular Probes) with quoted free Ca^{2+} concentrations in the range of 17 nM to 39 μM . Several fluorescence decay curves measured in the two-photon excitation regime are shown in Fig.2(a). The fluorescence lifetimes were obtained from the numerical analysis of these data.

Thorough numerical fit must take into account the IRF of the system.⁸ As opposed to conventional systems with strongly asymmetric IRF, the Gaussian-like IRF of our system assumes a simple analytical expression for the measured fluorescence decay. Thus, for a train of excitation pulses of period T , each term of a multi-exponential decay process reads

$$I_j = \frac{1}{2} \left[\frac{1 + e^{-T/\tau_j}}{1 - e^{-T/\tau_j}} - \text{erf} \left(\frac{\sigma_{\text{IRF}}}{\sqrt{2}\tau_j} - \frac{t}{\sqrt{2}\sigma_{\text{IRF}}} \right) \right] \times \exp \left(-\frac{t}{\tau_j} + \frac{\sigma_{\text{IRF}}^2}{2\tau_j^2} \right), \quad j = \{f, i, s\} \quad (1)$$

where a triple-exponential decay is assumed and index j indicates fast (f), intermediate (i) and slow (s) temporal components, τ_j is the fluorescence emission lifetime ($\tau_f < \tau_i < \tau_s$) and $\text{erf}(z) = \frac{2}{\sqrt{\pi}} \int_0^z \exp(-\xi^2) d\xi$ is the error function. Eq.(1) takes the periodic train of excitation pulses and response time jitter of the SPAD into account, such that our data in Fig.2 do not require deconvolution processing.

Analysis of the OGB-1 fluorescence reveals the best agreement with a triple exponential decay approximation. The data are modeled using the function $A_f I_f + A_i I_i + (1 - A_f - A_i) I_s$ with the fast $I_f(t)$, intermediate $I_i(t)$ and slow $I_s(t)$ decaying components (1) of normalized partial intensities A_f , A_i and $A_s = 1 - A_f - A_i$, respectively. Fig.2 details a comparison between the double- (magenta) and triple-exponential (wine curve) models applied to fluorescence from a 38 nM Ca^{2+} concentration sample (red points and curve). In both cases, the residues [Fig.2(b)] do not show any bias that might be caused by the Gaussian curve approximation of the IRF, while the accuracy of the numerical fit is improved in case of the triple-exponential model. Wilms et al.⁸ have made the same observation for OGB-1 fluorescence in the absence of Ca^{2+} . However, it was attributed to contaminating dye derivatives and a double-exponential model has been utilized for samples containing Ca^{2+} . Note that at high Ca concentration, large

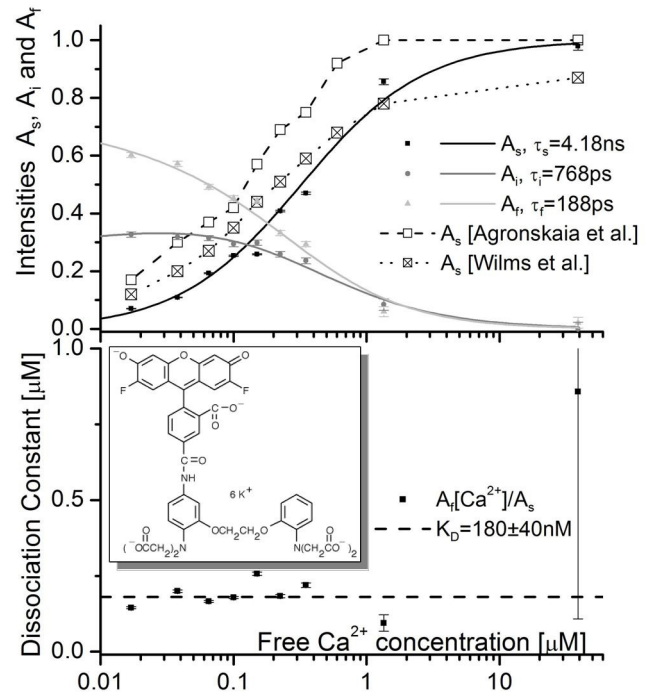


FIG. 3: Top panel: Partial intensities of the slow (A_s), intermediate (A_i) and fast (A_f) decay components of OGB-1 fluorescence as a function of the free Ca^{2+} concentration. The lifetimes are 4.18 ± 0.01 ns, 768 ± 16 ps and 188 ± 6 ps. Our data are shown in comparison with the data from [7] and [8]. The numerical fit to the model (2) (curves) yields $K_D = 195 \pm 9$ nM, $K_{Dn} = 4 \pm 6$ μM and $n = 9 \pm 3$. Bottom panel: The ratio $A_f[\text{Ca}^{2+}]/A_s$ (points) and its average yielding $K_D = 180 \pm 17$ nM (curve). The case of the Ca^{2+} -saturated buffer is excluded from the average because of the large error caused by A_f approaching null. The inset shows the OGB-1 molecule structure

amplitude of long leaving component make difficult the fit of short lifetime components with small amplitudes. Previously reported data^{1,7,8} for OGB-1 fluorescence lifetimes thus assume the double-exponential decay approximation. We argue that PMT-based systems used so far exhibit insufficient temporal resolution to enable observation of the triple-exponential behavior.

Using triple-exponential fluorescence decay (1) with the lifetimes independent of the calcium buffer,^{1,8} we applied a global numerical analysis to our data, yielding the partial intensities A_f , A_i and A_s in function of free Ca^{2+} concentration (Fig.3). Temporal resolution of our system allows the short lifetime component ($\tau_f \sim 190\text{ ps}$) to be unambiguously resolved in the background of the intermediate- and long-living fluorescence ($\tau_i \sim 770\text{ ps}$ and $\tau_s \sim 4.2\text{ ns}$). The partial intensities A_f and A_i decrease while the slow-component intensity $A_s = 1 - A_f - A_i$ increases with concentration [Ca^{2+}] (top panel).

We attribute, as usual, the short- and long-lifetime components to, respectively, unbound and Ca^{2+} -bound OGB-1 with a simple 1:1 complex stoichiometry. As such and because the intensities are defined by complex concentrations,

we obtain that $A_f \propto [D]$ and $A_s \propto [CaD] = K_D^{-1} [Ca^{2+}][D]$ with $[D]$ and $[CaD]$ being the unbound and Ca-bound OGB-1 concentrations and K_D the dissociation constant of the 1:1 complex. Respectively, the ratio $A_f[Ca^{2+}]/A_s$ yields an estimate of the dissociation constant $K_D = 180 \pm 17$ nM, in good agreement with the quoted value 170 nM (Fig. 3, bottom panel).

In Fig.3, the long lifetime component A_s is in good agreement with the measurements of Agronskaia⁷ and Wilms,⁸ but in [8], A_s is less than one in Ca^{2+} -saturated buffer and an apparent K_D is too high (~ 300 nM). These discrepancies are attributed to the dye impurities and to the difference in two-photon absorption cross-sections of Ca-bound and unbound OGB-1, which are said⁸ difficult to be quantified.

For the Ca-bound OGB-1, Lakowicz¹ reported τ_s of 4 ns, which well agrees with our data. In [7], τ_s varies in the range 2.6-3.7 ns, while in [8], $\tau_s = 3.63$ ns. For the Ca-free OGB-1, a single lifetime component τ_f has been measured of 700 [1], 290-420 [7] and 346 ps [8], respectively. These results correspond to the combined effect of the decay processes with the lifetimes $\tau_f \sim 190$ ps and $\tau_i \sim 770$ ps in our measurements, which may not have been resolved in previous studies. The experimental setup in [8] relies on a commercially available PMT with a quoted timing jitter of 200 ps. Other data^{1,7} are reported without timing resolution of experimental setups.

Due to the Ca-binding features of the octadentate chelator BAPTA,¹⁴ the 1:1 stoichiometry is usually attributed to the Ca-bound Oregon Green BAPTA-1 as well. However, the molecule of OGB-1 has an asymmetric structure with respect to its BAPTA moiety (Fig.3, inset). The asymmetric arrangement of the carboxyl functional groups, benzol rings, fluorine and nitrogen atoms as well as the variations of electronic density from low (at hydrogen in carboxyl groups) to high (at benzol rings, F and O atoms) assume a polarity of the molecule and, as a consequence, weak dipole-dipole intermolecular forces. As a result of such interaction forces, several OGB-1 molecules might be coordinated to a Ca-bound OGB-1 forming thus a polymolecular association with a calcium:indicator molar ratio 1:n. The intermediate lifetime component τ_i in Fig. 3 then might be attributed to such polymolecular association, yielding $A_i \propto [Ca_{1/n}D] = K_{Dn}^{-1/n} [D][Ca^{2+}]^{1/n}$ with K_{Dn} being the corresponding dissociation constant. Note that for-

mation of a polymolecular structure is a very complex processes and requires thorough investigations but a non 1:1 stoichiometry of Ca:OGB-1 has been reported in Ref.15 and here it allows us to build the accurate model:

$$\frac{[Ca^{2+}]}{K_D} = \frac{A_s}{A_f} = \frac{A_s}{1-A_s} \left[1 + \frac{A_i}{A_f} \right], \quad \frac{[Ca^{2+}]}{K_{Dn}} = \left(\frac{A_i}{A_f} \right)^n. \quad (2)$$

In the limit $K_{Dn} \rightarrow \infty$ (double exponential decay), it agrees with the Hill equation, as opposed to the model in Ref. [8]. The numerical fit of data in Fig.3 reports small binding affinity ($K_{Dn} \sim 4 \mu M$) and $n=9$ indicating the most probable form of polymolecular association with eight Ca-free molecules coordinated to the Ca-bound OGB-1. The dissociation constant K_D reported by the fit is 195 nM, in agreement with the average of $A_f[Ca^{2+}]/A_s$ (bottom panel).

For the first time, the triple exponential fluorescence in non-ratiometric Ca probes as an effect of dye contaminations was suggested by Lakowicz⁹ for the Calcium Green (CG-1). The CG-1 molecule has the same structure as OGB-1 but the two F atoms are replaced by Cl, yielding $\tau_f = 50$ ps, $\tau_i = 450$ ps and $\tau_s = 3.7$ ns. Interestingly, the signature of non-1:1 stoichiometry has been noticed for Ca-bound CG as well.¹² We find that at low Ca^{2+} concentration, the ratio $A_f[Ca^{2+}]/A_s$ in [9] is a constant of 170 ± 20 nM, yielding K_D close to the quoted value of 190 nM. (The K_D obtained by Lakowicz using a conventional model¹³ is 128 nM). At high Ca concentration, the band pass of the system (2GHz modulation using a frequency-domain FLIM technique) was insufficient to accurately measure the small component A_f . The data of Ref.[9] can thus be accurately interpreted in the framework of our model (2), without appealing to dye impurities.

In summary, we have shown that high-temporal resolution measurements of the triple-exponential fluorescence decay of non-ratiometric Ca^{2+} indicators allow the free Ca^{2+} concentration and dye dissociation constant to be measured precisely.

DLB is grateful to Leonid Zekel for discussions on the model. This research was supported, in part, by a grant of the Swiss National Science Foundation and by Centre SI of EPFL.

* Electronic address: dmitri.boiko@csem.ch

¹ J. Lakowicz, *Principles of Fluorescence Spectroscopy*, Plenum, New York (1999)

² K. Suhling, P.M.W French and D. Phillips, *Photochem. Photobiol. Sci.* **4**, 13(2005)

³ D.V. O'Connor and D. Phillips, *Time-correlated Single Photon Counting*, Academic Press, London (1984)

⁴ S. Cova, A. Longoni, A. Andreoni and R. Cubeddu, *IEEE J. Quantum Electron.* **19**, 630(1983)

⁵ A. Gulinatti, P. Maccagnani, I. Rech, M. Ghioni and S. Cova, *Electron. Lett.* **41**, 272 (2005)

⁶ C. Niclass, A. Rochas, P.A. Besse, and E. Charbon, *IEEE J. Solid-State Circuits* **40** 1847(2005).

⁷ A.V. Agronskaia, L. Tertoolen and H.C. Gerritsen, *J. Biomed. Opt.* **9**, 1230(2004)

⁸ C.D. Wilms, H. Schnidt and J. Eilers, *Cell Calcium* **40**, 73(2006)

⁹ J. R. Lakowicz, H. Szmajnski, and M.L. Johnson, *J. of Fluorescence* **2**, 47 (1992)

¹⁰ W. Denk, J.H. Strickler and W.W. Webb, *Science* **248**, 73(1990)

¹¹ A. Habenicht, J. Hjelm, E. Mukhtar, F. Bergstrom and L.B.A. Johansson, *Chem. Phys. Lett.* **354**, 367(2002)

¹² M. Eberhard and P. Erne, *Biochem. and Biophys. Res. Comm.* **180**, 209 (1991)

¹³ G. Grynkiewicz, M. Poenie, and R. Y. Tsien, *J. Biol. Chem.* **260**, 3440 (1985)

¹⁴ R. Y. Tsien, *Biochemistry* **19**, 2396 (1980)

¹⁵ D. Thomas, S.C. Tovey, T.J. Collins, M.D. Bootman, M. J. Berridge, P. Lipp, *Cell Calcium* **28**, 213 (2000)